Microbial Reduction of Fe(III) in Hematite Nanoparticles by Geobacter sulfurreducens

ARTICLE *in* ENVIRONMENTAL SCIENCE AND TECHNOLOGY · OCTOBER 2008

Impact Factor: 5.33 · DOI: 10.1021/es800620f · Source: PubMed

Environ. Sci. Technol. **2008,** *42,* 6526–6531

Microbial Reduction of Fe(III) in Hematite Nanoparticles by *Geobacter sulfurreducens*

BEIZHAN YAN,[†] BRIAN A. WRENN,[‡] SOUBIR BASAK, PRATIM BISWAS, AND DANIEL E. GIAMMAR*

Department of Energy, Environmental, and Chemical Engineering and Center for Materials Innovation, Washington University in St. Louis, Missouri 63130

Received March 1, 2008. Revised manuscript received June 12, 2008. Accepted June 14, 2008.

The rates of microbial Fe(III) reduction of three sizes of hematite nanoparticles by *Geobacter sulfurreducens* were measured under two H_2 partial pressures (0.01 and 1 atm) and three pH (7.0, 7.5, and 8.0) conditions. Hematite particles with mean primary particle sizes of 10, 30, and 50 nm were synthesized by a novel aerosol method that allows tight control of the particle size distribution. The mass-normalized reduction rates of the 10 and 30 nm particles were comparable to each other and higher than the rate for the 50 nm particles. However, the surface area-normalized rate was highest for the 30 nm particles. Consistent with a previously published model, the reduction rates are likely to be proportional to the bacteria−hematite contact area and not to the total hematite surface area. Surface area-normalized iron reduction rates were higher than those reported in previous studies, which may be due to the sequestration of Fe(II) through formation of vivianite. Similar initial reduction rates were observed under all pH and H_2 conditions studied.

1. Introduction

The redox cycling of Fe plays pivotal roles in biogeochemical cycles in natural environments. Redox transformations of Fe(III) oxides and oxyhydroxides, which are strong adsorbents for many metals and metalloids, can affect the environmental fate and transport of contaminants (*1*). Fe(III) reduction produces Fe(II), which is an effective reductant when present at Fe(III) oxide surfaces. Contaminants that are amenable to surface-mediated reduction by solid-associated Fe(II) include chlorinated aliphatic and nitroaromatic hydrocarbon compounds (*2, 3*) and certain heavy metals and radionuclides (*4–6*).

In soil and sediment environments, Fe oxides and oxyhydroxides can be present as amorphous materials or as well-crystallized minerals such as hematite (α-Fe_2O_3) and goethite (α-FeOOH) (*7, 8*). The presence of Fe oxide and oxyhydroxide nanoparticles in natural systems has been recognized relatively recently (*9*). Such nanoparticles can be formed in environments with large geochemical gradients that promote supersaturation and rapid nucleation, such as those occurring during the rapid enzymatic oxidation of Fe(II) by bacteria (*9*). In addition to their abundance in many environments, Fe oxide nanoparticles may be added to environmental systems to enhance biogeochemical processes for contaminant degradation or immobilizaton. The addition of Fe oxide nanoparticles could augment the available Fe(III) in contaminated environments to allow greater contaminant reduction by microbially produced Fe(II).

The biogeochemical cycling of iron is mediated by biological processes involving Fe(II)-oxidizing and Fe(III)-reducing microorganisms (*10*). The dissimilatory microbial (enzymatic) reduction of Fe(III) minerals is an important terminal electron accepting process in many anaerobic environments (*4*), and iron reducing bacteria (IRB) can control contaminant transformation and transport in the subsurface (*11*). *Shewanella*, a facultative IRB genus, has been extensively studied (*12–14*). In natural anaerobic environments, the IRB *Geobacter* is more abundant and plays an important role in the reduction of Fe(III) (*15*). *Geobacter sulfurreducens*, the bacteria used in the present study, has been found in various settings including several contaminated subsurface sites (*4, 15, 16*).

Recent studies have examined the effect of Fe oxide structure and size on microbially mediated Fe(III) reduction rates. Roden (2003) observed a strong linear correlation of the initial rate of microbial Fe reduction and oxide surface area and suggested that bacterial Fe(III) reduction does not respond strongly to oxide crystal thermodynamic properties (*17*). In contrast, Bonneville et al. (2004) suggested that solubility appears to be the rate-controlling factor in both biotic and abiotic reduction of Fe(III) oxyhydroxides (*18*). In these two studies as well as other previous work (*19, 20*), identifying effects of particle size on reduction rates has been elusive because comparative experiments either investigated different mineral phases or examined the same mineral over a limited range of particle sizes (*20*). The determination of size effects on reduction rates of nanoparticles requires systematic investigation of the same crystalline phase in different sizes.

Due to their high specific surface areas, nanoparticles exhibit enhanced reactivity per unit mass with respect to compositionally identical materials in larger grain sizes. However, reaction rates will only scale with the available reactive surface area, which may be different from the total surface area of the primary particles, especially if particles are present as aggregates (*19*). In addition to the effect of size on particle surface area, nanoscale size may also affect the structure and reactivity of particles. Size effects may give rise to nanoparticles that are more soluble (*21*) or less soluble (*22*) than coarser particles.

To investigate nanoscale size effects on the kinetics of microbial iron reduction, this study used hematite nanoparticles with mean primary particle sizes of 10, 30, and 50 nm. The objectives of the present study were to determine the effects of particle size, concentration of electron donor (H_2), and pH on the rate and extent of the microbial reduction of Fe(III) in hematite.

2. Experimental Section

Synthesis of Hematite Nanoparticles. Hematite particles were synthesized by a gas phase method that allowed tight control of particle composition and size (Figure 1). A bubbler with a flow of N_2 (0.3−200 cm^3/min) at 30 °C was used to introduce a precursor of iron pentacarbonyl into a furnace aerosol reactor (FuAR) (Lindbergh BlueM model STF54779C).

* Corresponding author phone: (314)-935-6849; fax: (314)-935-7211; e-mail: giammar@wustl.edu.

[†] Current address: Lamont-Doherty Earth Observatory of Columbia University, 61 Rt. 9W, Palisades, NY 10964.

[‡] Current address: The National Corn-to-Ethanol Research Center, 400 University Park Dr., Edwardsville, Illinois 62026.

10.1021/es800620f CCC: $40.75
Published on Web 07/22/2008

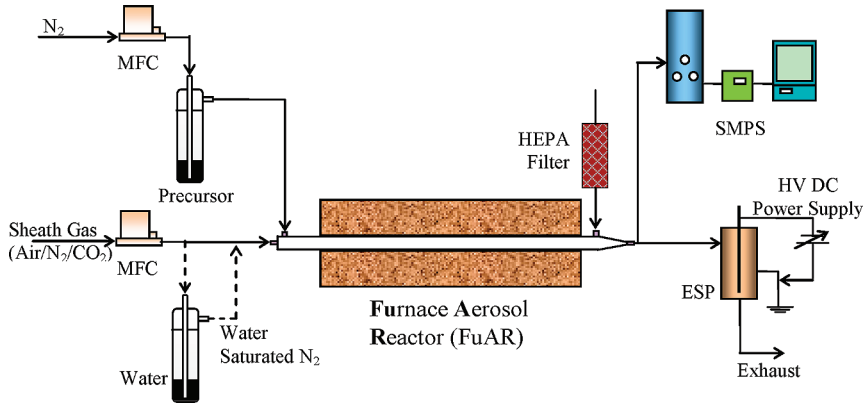

FIGURE 1. System for aerosol-based synthesis of hematite. Mass flow controllers (MFC) control flows into the furnace aerosol reactors. Exiting particles are captured in an electrostatic precipitator (ESP) and in-flight size distributions are determined with a scanning mobility particle sizer (SMPS).

The precursor decomposes in the FuAR at temperatures from 1000−1200 °C. A sheath gas of air was used (3−20 L/min) as the oxidant and to control the residence time inside the reactor. A diluter system quenched the temperature of the exhaust gas coming out of the reactor. A cylindrical electrostatic precipitator was used to collect the particles using +12 kV applied potential. Precursor flow rate, decomposition temperature, and furnace residence time are key factors that control the size and crystallinity of the nanoparticles (*23*). The synthesized particles were characterized by size distribution analysis, scanning and transmission electron microscopy, and X-ray diffraction. The mobility-based particle size distribution was measured in flight using a scanning mobility particle sizer that consisted of a differential mobility analyzer and a condensation particle counter. Because in-flight particles consisted of agglomerates, the size distributions of primary particles were determined by electron micrograph image analysis. Particle size distributions were narrower than those from aqueous syntheses (*24*), and the very rapid nucleation during gas-phase synthesis may result in different surface structures than from aqueous syntheses. Details regarding the synthesis method, size distributions (Table S1 and Figure S1), morphology (Figure S2, electron microscopy), and phase identity (Figure S3, X-ray diffraction) are included in the Supporting Information.

Iron Reduction by *Geobacter sulfurreducens*. Standard anaerobic techniques were used throughout the experiments. Gases (N_2, H_2, or N_2+CO_2 mixture) were passed through a column of hot copper mesh to remove any traces of O_2. Transferring and sampling of microbial cultures were performed with syringes and needles that had been flushed ten times with the O_2-free gas. The transfer of cells to centrifuge tubes for cell washing was performed in an anaerobic chamber with a 95% N_2 and 5% H_2 atmosphere that was recirculated though a heated palladium catalyst.

A culture of *Geobacter sulfurreducens* was purchased from the American Type Culture Collection. Growth medium was prepared with the following constituents in 1 L of ultrapure (resistivity >18.2 MΩ-cm) water: 2.5 g of $NaHCO_3$, 0.1 g of KCl, 0.25 g of NH_4Cl, 0.6 g of $NaH_2PO_4 \cdot H_2O$, Wolfe's vitamin and trace mineral solutions (10 mL each), and 1 mL of 1 mM Na_2SeO_4. Sodium acetate (3.4 g/L) and sodium fumarate (8.0 g/L) were used as the electron donor and electron acceptor for cell growth. After sparging the solution with the N_2/CO_2 (80:20 v:v) gas mixture, the pH of the medium was ∼7.0.

For hematite reduction experiments, bacteria were harvested in the late-lag growth phase and washed three times with bicarbonate-buffered ultrapure water (pH 6.8). The reaction medium contained 30 mM HEPES as a pH buffer, 10% of the major constituents of the growth media, Wolfe's vitamins and trace minerals solutions (10 mL each), and 1 mL of 1 mM Na_2SeO_4. The concentrations of major constituents in the reaction media provided sufficient nutrients to maintain the cells' biological function and cell density but were insufficient for cell growth.

To start microbial Fe(III) reduction experiments, washed cells were added to hematite suspensions in anaerobic reaction media to provide final cell densities from 2×10^7 to 2×10^8 cells/mL. Glass culture tubes with gastight butyl rubber septa were used to maintain anaerobic conditions. The final hematite concentration in the reaction media was 0.15 g/L. A volume of H_2 calculated to achieve a certain partial pressure of H_2 was added to the head space of each reaction tube. Reaction tubes were continuously mixed on a rotary shaker at 32 °C, and samples were periodically collected for measuring cell density and Fe(II) concentration.

Two sets of experiments (short-term and long-term) were conducted. The short-term set was designed to examine the initial reduction rate as a function of particle size, H_2 partial pressure, and pH. Samples were collected at 1, 2, 4, 8, 12, 24, and 72 h. The long-term experiments were used to assess the overall extent of Fe(III) reduction after three months. To minimize the interference that may be introduced by intensive sampling during the first days of an experiment, samples were collected every three days for the first two weeks and then once every week for the remaining three months. A constant H_2 partial pressure was maintained throughout each experiment by adding the necessary volume of H_2 to the reactor after each sampling event.

Cell growth prior to addition of nanoparticles was monitored by directly inserting the culture tubes into a colorimeter (Hach D/R 850) and measuring the absorbance at 540 nm. During the microbial reduction experiments with hematite nanoparticles present, the cell density in the reaction solution was monitored by analyzing the protein concentration with Pierce BCA (bicinchoninic acid) Protein Assays (*25*). In the protein analysis, 0.5 mL samples were washed using bicarbonate-buffered solution, and then 0.2 mL of 0.1 M NaOH was added to extract protein. Samples were heated at 90 °C in a water bath for 20 min. After centrifugation at 8000*g* for 20 min, the supernatant was used for protein analysis. The cell density and pH were measured at the conclusion of each experiment; pH did not vary by more than 0.2 pH units, and the cell density decreased by less than 20%.

Fe(II) Measurement. A modified ferrozine method was used to determine the Fe(II) concentration. Ferrozine forms a colored complex with Fe(II) that can be measured colorimetrically (*26*). At each of the sampling points, the concentration of 0.5 N HCl-extractable Fe(II) was measured. Concentrations of three pools of Fe(II) were measured at the end of the experiments: soluble, 0.5 N HCl- and 3 N HCl-

extractable Fe(II). The soluble Fe(II) concentration was determined as that in the filtrate that passed a 0.025 μm filter. To determine 0.5 and 3 N HCl-extractable Fe(II) concentrations, specific volumes of HCl were added to unfiltered samples and mixed for 24 h. The acidified samples were centrifuged, and then supernatants were transferred to 3 mL of ferrozine solution. The pH was adjusted to 7 by addition of NaOH and the solution was filtered to remove possible Fe(III) precipitates. The absorption at 562 nm was measured for quantification of the Fe(II) concentration. In the samples for which all three Fe(II) pools were measured, soluble Fe(II) was always less than ~10% of the HCl-extractable Fe(II), while 0.5 N HCl-extractable Fe(II) was within 5% of the value of the 3 N HCl-extractable Fe(II). Secondary minerals that formed during microbial reactions and were visible without magnification could be dissolved in both 0.5 and 3 N HCl. Comparable Fe(II) levels in both solutions indicated that complete Fe(II) extraction was achieved with 0.5 N HCl. In this paper, 0.5 N HCl-extractable Fe(II) levels are reported for ease of comparison with other studies (*27–29*).

Spectroscopic Analysis and Electron Microscopy. To observe the spatial relationship of cells and minerals, aliquots of suspensions from the experiments were filtered with 0.2 μm PCTE membranes (GE Osmonics). Glutaraldehyde (2.5%) and osmium tetroxide (1%) were used to fix the bacteria on the filter, and the fixed samples were then dehydrated in an increasingly graded series of ethanol. The samples were further prepared using critical point drying with CO_2. Mounted samples were sputter-coated with 50 nm of gold and examined in a Hitachi S-450 scanning electron microscope (SEM) operated at 20 kV accelerating voltage.

To better determine the composition of secondary phases that formed during the reactions, the inorganic solids were separated from cells and analyzed by SEM and Fourier transform infrared spectroscopy (FTIR). The dark gray particles were allowed to settle in the reaction tubes for 15 min, and the supernatant, which contained most cells, was then removed. The settled particles were washed three times with bicarbonate-buffered ultrapure water, collected on a 0.2 μm filter membrane, dried in an anaerobic chamber, and stored under anoxic conditions prior to analysis. The size and microstructure of the collected solids were analyzed with a Hitachi S4500 SEM, and the elemental composition was analyzed by energy dispersive X-ray (EDX) spectroscopy. Samples for SEM were prepared on support film grids (Lacey Formvar/Carbon, 200 mesh, Copper; Ted Pella Inc.). FTIR (Thermo Nicolet Nexus 470) was performed using a germanium attenuated total reflectance accessory for analysis of solid samples. Solids present on the filter were pressed directly onto the germanium crystal. Because the solids analyzed had been separated from the majority of the biomass, their IR spectra have little interference from organic compounds.

3. Results and Discussion

Rate and Extent of Microbial Iron Reduction. Initial reduction rates for the first 24 h were quantified by the linear fit to the Fe(II) concentrations at the conditions of 2.30×10^7 cells/mL and pH 7 (Figure 2a). The linear relationship indicates a relatively constant rate of Fe(III) reduction over the reaction period. Fe(II) concentrations from reaction of 10 and 30 nm hematite are similar throughout the course of the reaction and are 1.5−2.7 times higher than those from reaction of the 50 nm particles (Table 1). The reduction rates of the 10 and 30 nm hematite were ~0.8 mg/L·h, leading to a reduction of ~17% of the total Fe(III) in the first 24 h. The 50 nm particles were reduced at a slower rate (~0.35 mg/L·h) and only 6% of the Fe(III) was reduced. The reduction rates of the 30 and 10 nm hematite particles were also similar to one another at a higher cell density (1.9×10^8 cells/mL) at pH 7.5 (Figure 2b). Compared to the constant rates observed when the lower cell density was used, the reduction rates of 10 and 30 nm hematite particles decreased with time when the high cell density was used. Although initial rates of Fe(II) production were nearly twice as fast as in the low cell density sets, the amounts of Fe(II) produced in the first day were similar for the two sets.

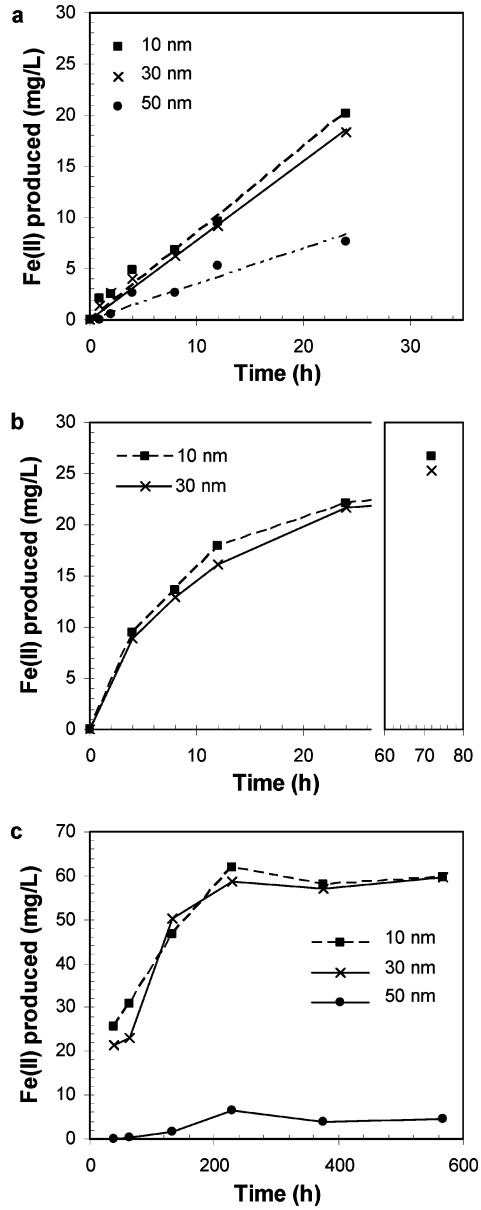

FIGURE 2. Production of Fe(II) in (a) short-term experiments with a low cell density (~2.3 × 10^7 cells/mL), 150 mg/L hematite, pH 7.0, and 1 atm H_2, (b) short-term experiments with a high cell density (~1.9 × 10^8 cells/mL), 150 mg/L hematite, pH 7.5, and 1 atm H_2, and (c) long-term experiments at pH 7.5, 150 mg/L hematite, cell density of 1.0 × 10^8 cells/mL, and 1 atm H_2 pressure. For (a) the lines are linear fits to the data representing Fe(II) production rates of 0.84 mg/L·h (10 nm), 0.77 mg/L·h (30 nm), and 0.35 mg/L·h (50 nm). A hematite concentration of 150 mg/L corresponds to 105 mg/L Fe(III).

In the long-term experiments, Fe(II) concentrations steadily increased for one week and then leveled off (Figure 2c). Similar to the observation in short-term experiments, the 10 and 30 nm nanoparticle samples have comparable Fe(II) concentrations throughout the reactions that are higher than those for the 50 nm samples. The final concentrations

TABLE 1. Hematite Nanoparticles Investigated and Their Reduction Rates at pH 7, 1 atm P_{H2}, $\sim 2.3 \times 10^7$ cells/mL, and 0.15 g/L hematite (0.105 g/L Fe(III))

particle label	particle diameter [a](nm)	specific surface area [b](m^2/g)	mass-normalized reduction rate (mg/L·h)	surface area-normalized reduction rate (nmol/m^2·h)	surface area and cell density-normalized reduction rate (nmol·L/m^2·h·10^8cell)
10 nm	9.5 ± 1.4	119.8	0.84	837	3.60
30 nm	29.4 ± 1.6	40.4	0.77	2280	9.78
50 nm	51.4 ± 1.7	21.1	0.34	1920	8.26

[a] Geometric mean primary particle size and standard deviation estimated from electron micrograph (SEM/TEM) analysis. [b] Surface areas are calculated under the assumption that hematite particles are spheroid and have a particle size distribution as measured during synthesis.

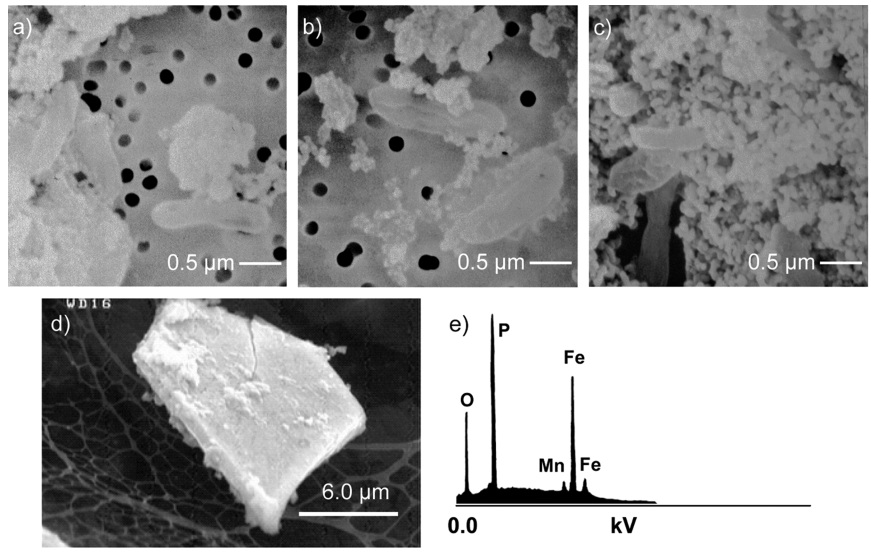

FIGURE 3. Scanning electron micrographs of cells of *Geobacter sulfurreducens* and aggregates of (a) 10 nm, (b) 30 nm, and (c) 50 nm hematite particles on 0.2 μm filter membranes and (d) particles collected following microbial reduction of the 30 nm hematite, and (e) the associated EDX spectrum.

are 55−60 mg/L for the 10 and 30 nm particles and 5−8 mg/L for the 50 nm particles.

When normalized to particle surface area, the highest reduction rate is for the 30 nm particles (Table 1). The specific surface area of the 10 nm hematite is 119.8 m^2/g, which is 3−6 times larger than the areas of the 30 and 50 nm particles; however, the mass-normalized reduction rate of the 10 nm hematite is similar to that of the 30 nm hematite and merely 2.5 times higher than that of the 50 nm particles. Particle aggregation can alter the available reactive surface area of the particles and thereby affect the reaction rate. Roden (2003) observed that feroxyhyte and ferrihydrite, which had specific surface areas of 176 and 290 m^2/g, respectively, had mass-normalized Fe(III) reduction rates similar to those of goethite particles (30−100 m^2/g) that did not scale with surface area (*17*). He suggested that particle aggregation was a major reason to cause the relatively low reduction rates of feroxyhyte and ferrihydrite. In the current study, aggregation of the particles was observed, which can reduce the difference in their available surface areas and lead to comparable mass-normalized reduction rates. Sonication of the suspensions was used to disperse the hematite particles before addition of cells, but after sonication was stopped the particles visibly reaggregated within a half-hour in both experiment and control samples. In contrast to the 10 and 30 nm particles, the 50 nm particles were contained within permanently aggregrated structures of approximately 200 nm that could not be dispersed by sonication (Figure S2 of Supporting Information).

The higher surface area-normalized Fe(III) reduction rate of 30 nm than of 10 and 50 nm hematite particles may also be due to particle aggregation. The relative decrease in the effective surface area caused by aggregation was likely greater for the 10 nm particles than for the 30 nm particles, and the more fixed aggregate structure of the 50 nm particles would limit its effective surface area. Such differences in relative decreases in effective surface area may partially explain the higher surface area-normalized rate of 30 nm observed in this study. Bonneville et al. (2006) found that the reduction rate correlated linearly with the relative coverage of the cell surface of *S. putrefaciens* by nanohematite particles (*19*). Accordingly, aggregation of particles will decrease their coverage of cell surfaces (Figure 3a−c). Because Fe(III) reduction by *Geobacter sulfurreducens* occurs at the outer cell membrane (*30*), the reduction rates should not be expected to be correlated with total particle surface area but rather with the area of particle-bacteria contact.

The rate of microbial reduction of the 10 nm hematite particles was not significantly affected by the partial pressure of H_2 or the pH over the limited range of conditions studied. The extent of reduction after 64 h with 0.01 atm P_{H2} was very similar to that with 1.0 atm P_{H2} for all three pH values studied (Figure 4). The headspace was large enough that available H_2 would be sufficient for complete hematite reduction even at 0.01 atm P_{H2}. The independence of the reaction rate with respect to P_{H2} indicates that the transport of H_2 to the cells is not a rate-determining step, which is consistent with previous research (*31*). Over the pH range studied, the reduction rate is not significantly affected by pH (Figure 4). Regardless of the pH and H_2 pressure, the final Fe(II) iron concentration in long-term experiments (3 months) always reached 60−65 mg/L, indicating that the H_2 and pH were not controlling factors of the overall extent of iron reduction.

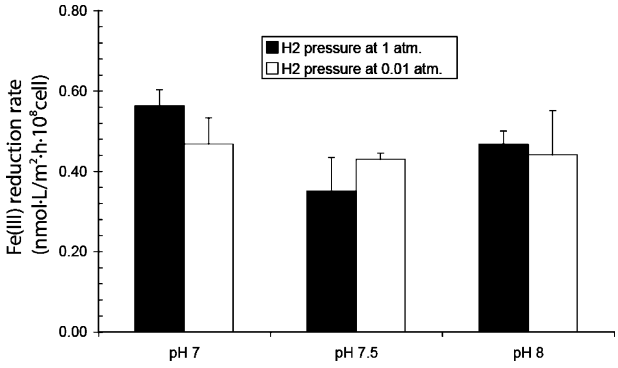

FIGURE 4. Iron reduction rates of 10 nm hematite particles in the first 64 h at different pH and H_2 conditions. The results are the means of triplicate experiments. Error bars designate one standard deviation.

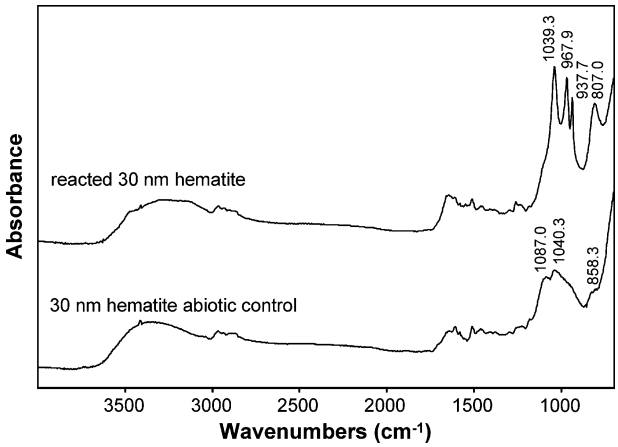

FIGURE 5. FTIR spectra of mineral solids remaining after 3 months of reaction of 30 nm hematite in the long-term experiments.

Formation of Secondary Minerals. Secondary mineral formation was first indicated by a visible change in the color of the reaction suspension that accompanied the production of Fe(II). For the 10 and 30 nm particles, the solution color changed from red, which was derived from hematite particles, to gray. The color of the 50 nm particle suspensions remained the same red color throughout the experiments.

Several lines of evidence indicate that vivianite ($Fe_3(PO_4)_2 \cdot 8H_2O$), a colorless mineral, was produced. Figure 5 shows ATR-FTIR spectra of inorganic solids from suspensions before and after microbial reduction of 50 nm hematite. Absorbance peaks at 938, 968, and 1039 cm^{-1} observed in samples following reaction of 10 and 30 nm particles are consistent with those for P−O stretching (*32*). For 50 nm samples, these peaks are present but are much weaker, indicating that phosphate was less abundant in these samples. No peaks corresponding to a carbonate mineral such as siderite were observed. SEM-EDX imaging and analysis was used to investigate the morphology and chemical composition of the secondary phases. The secondary solids have distinctive pinnacoid and bladed morphology, which is consistent with vivianite, and are much larger (~0.5 to 10 μm) than the hematite particles (Figure 3d). These larger particles were more abundant in samples from reaction of the 10 and 30 nm hematite than of the 50 nm hematite. This observation is consistent with the lower Fe(II) concentrations and weaker IR absorbance from P−O stretching from solids from experiments with the 50 nm hematite. EDX analysis of these μm-scale minerals identified Fe and P as major constituent elements (Figure 3e). Vivianite has also been observed in previous iron reduction experiments (*1*).

Rapid Reduction of Iron(III) in Hematite Nanoparticles. The surface area-normalized iron reduction rates of 837−2280 nmol/$m^2 \cdot$h measured in this study (Table 1) are higher than those in other studies using hematite as the electron acceptor. The fast rate reported in this study is statistically meaningful because all reported data are the average of three samples with a standard deviation less than 15%. An average hematite reduction rate of 260 nmol/$m^2 \cdot$h from two different studies is summarized by Roden (2003) (*17*); however, these studies were for *Shewanella* species and not for *Geobacter*. Although direct comparisons of results from different studies are not possible because of differences in the Fe(III) oxide, microorganism, and electron donor, a general comparison of the magnitude of the rate with previous studies is illustrative. For hydrous ferric oxide reduction with acetate as the electron donor, a rate of 380 nmol/$m^2 \cdot$h was measured for reduction by *Geobacter sulfurreducens* (*33*) and of 26 nmol/$m^2 \cdot$h by *Geobacter metallireducens* (*34*). Because the nanoparticles in the current study were synthesized from the gas phase, the Fe(III) in the near-surface region of the particles may have been more disordered and more bioavailable than the Fe(III) in the core of the particles, which may have contributed to the relatively high initial reduction rates.

The removal of Fe(II) from solution by precipitation instead of by adsorption to particle and cell surfaces can contribute to the rapid initial iron reduction rates. Previous research has found that the sorption and/or surface precipitation of Fe(II) to surfaces of bacteria (*35*) and Fe(III) minerals (*33*) inhibits iron reduction. In this study inhibition was not initially observed, and the precipitation of vivianite may have delayed the saturation of the hematite or bacteria surfaces with adsorbed Fe(II) and allowed more continuous Fe(III) reduction. Ultimately, once all available phosphate was consumed by vivianite formation, the reduction of hematite in this study may have been limited by Fe(II) adsorption to hematite. Some limit of Fe(II) production is evident from the leveling off of Fe(II) in long-term experiments. Other common Fe(II) minerals, magnetite and siderite, were not observed in this study. If all of the available phosphate was precipitated as vivianite, about 33% of total Fe could be precipitated in vivianite. Out of the total of 55% of the Fe that was reduced to Fe(II), this leaves ~22% of the total Fe as Fe(II) as either soluble or adsorbed species. After two months of reaction, soluble Fe was also only 10% of the total Fe, which indicates that about 12% of the total Fe is expected to be Fe(II) adsorbed to the surfaces of hematite and cells.

Environmental Implications. For application in environmental technologies, hematite particles should be small enough to be delivered to the subsurface and have high rates of reactions at surfaces. The smallest particles studied in this project have the highest mass-normalized rates of microbial Fe(III) reduction. Although the surface area-normalized rates may actually decrease with decreasing particle size, the overall higher Fe(II) production for small particles would still make them advantageous in environmental applications. Further, the smaller particles react more completely (e.g., 50% of the Fe in 10 and 30 nm nanoparticles was reduced, but less than 10% was reduced for 50 nm particles). In contrast to the strong effect of size on microbial reduction, the pH, cell density, and partial pressure of hydrogen had smaller or insignificant effects on microbial reduction.

The biogeochemistry of specific environments will determine the overall role of natural or engineered hematite nanoparticles in affecting contaminant fate and transport. As observed in this study, the presence of phosphate can cause vivianite precipitation and can drive iron(III) reduction faster by sequestering Fe(II). For the microbial production of Fe(II) to be useful in reducing oxidized contaminants (e.g.,

U(VI) and chlorinated aliphatic compounds), it is necessary that some Fe(II) adsorb to the surface of the iron oxides (*36*). However, even in the presence of vivianite, a previous study observed the reduction of Co(III) to Co(II) during Fe(III) reduction (*1*). The immobilization of metal and radionuclide contaminants will be affected by both adsorption and by surface-mediated reduction. For example, U(VI) species can adsorb to hematite, but reduction to U(IV) will immobilize the uranium more strongly.

The addition of hematite nanoparticles to contaminated subsurface systems can augment the iron-reducing capacity of the system. The delivery of nanoparticles will be affected by their deposition and transport properties. As observed in this work, very small nanoparticles can be present as much larger (micrometer-scale) aggregates, and it is this larger length-scale that may control transport.

Acknowledgments

This research was supported by a National Science Foundation Nanoscale Exploratory Research award (BES-0608749). We are grateful to Man J. Kwon and Kevin T. Finneran for their advice regarding the growth of *Geobacter sulfurreducens*. We appreciate the assistance of Edgar Leslie in Fe(II) analyses.

Supporting Information Available

Details of synthesis method and characterization of hematite nanoparticles (including 3 figures and Table 1). This material is available free of charge via the Internet at http://pubs.acs.org.

Literature Cited

(1) Zachara, J. M.; Fredrickson, J. K.; Smith, S. C.; Gassman, P. L. Solubilization of Fe(III) oxide-bound trace metals by a dissimilatory Fe(III) reducing bacterium. *Geochim. Cosmochim. Acta* **2001**, *65*, 75–93.

(2) Haderlein, S. B., III, Sparks D. L., Grundl, T. J. Eds.; Pollutant reduction in heterogeneous Fe(II)–Fe(III) systems. American Chemical Society: Washington, DC, 1999; Vol. 715, pp 342−356.

(3) Klupinski, T. P.; Chin, Y. P.; Traina, S. J. Abiotic degradation of pentachloronitrobenzene by Fe(II): Reactions on goethite and iron oxide nanoparticles. *Environ. Sci. Technol.* **2004**, *38*, 4353–4360.

(4) Lovley, D. R.; Holmes, D. E.; Nevin, K. P. Dissimilatory Fe(III) and Mn(IV) reduction. *Adv. Microbial Physiol.* **2004**, *49*, 219–286.

(5) Anderson, R. T.; Vrionis, H. A.; Ortiz-Bernad, I.; Resch, C. T.; Long, P. E.; Dayvault, R.; Karp, K.; Marutzky, S.; Metzler, D. R.; Peacock, A.; White, D. C.; Lowe, M.; Lovley, D. R. Stimulating the in situ activity of Geobacter species to remove uranium from the groundwater of a uranium-contaminated aquifer. *Appl. Environ. Microb.* **2003**, *69*, 5884–5891.

(6) Jeon, B. H.; Dempsey, B. A.; Burgos, W. D.; Barnett, M. O.; Roden, E. E. Chemical reduction of U(VI) by Fe(II) at the solid-water interface using natural and synthetic Fe(III) oxides. *Environ. Sci. Technol.* **2005**, *39*, 5642–5649.

(7) Cornell, R. M.; Schwertmann, U. The Iron Oxides; Wiley-VCH: Weinheim, Germany, 2003.

(8) Ehrlich, H. L. *Geomicrobiology*; Marcel Dekker, Inc.: New York, 2002.

(9) Banfield, J. F.; Zhang, H. Nanoparticles in the environment. In *Nanoparticles and the Environment*; Ribbe, P. H., Rossi, J. J. Eds.; The Mineralogical Society of America: Washington, DC, 2001; Vol. 44, pp 1−45.

(10) Lovley, D. R. Microbial Fe(III) reduction in subsurface environments. *FEMS Microbiol. Rev.* **1997**, *20*, 305–313.

(11) Wilkins, M. J.; Livens, F. R.; Vaughan, D. J.; Lloyd, J. R. The impact of Fe(III)-reducing bacteria on uranium mobility. *Biogeochemistry* **2006**, *78*, 125–150.

(12) Cooper, D. C.; Picardal, F. F.; Coby, A. J. Interactions between microbial iron reduction and metal geochemistry: Effect of redox cycling on transition metal speciation in iron bearing sediments. *Environ. Sci. Technol.* **2006**, *40*, 1884–1891.

(13) Behrends, T.; Van Cappellen, P. Competition between enzymatic and abiotic reduction of uranium(VI) under iron reducing conditions. *Chem. Geol.* **2005**, *220*, 315–327.

(14) Haas, J. R.; Dichristina, T. J. Effects of Fe(III) chemical speciation on dissimilatory Fe(III) reduction by *Shewanella putrefaciens*. *Environ. Sci. Technol.* **2002**, *36*, 373–380.

(15) Coates, J. D.; Phillips, E. J. P.; Lonergan, D. J.; Jenter, H.; Lovley, D. R. Isolation of Geobacter species from diverse sedimentary environments. *Appl. Environ. Microb.* **1996**, *62*, 1531–1536.

(16) Vrionis, H. A.; Anderson, R. T.; Ortiz-Bernad, I.; O'Neill, K. R.; Resch, C. T.; Peacock, A. D.; Dayvault, R.; White, D. C.; Long, P. E.; Lovley, D. R. Microbiological and geochemical heterogeneity in an in situ uranium bioremediation field site. *Appl. Environ. Microb.* **2005**, *71*, 6308–6318.

(17) Roden, E. E. Fe(III) oxide reactivity toward biological versus chemical reduction. *Environ. Sci. Technol.* **2003**, *37*, 1319–1324.

(18) Bonneville, S.; Van Cappellen, P.; Behrends, T. Microbial reduction of iron(III) oxyhydroxides: effects of mineral solubility and availability. *Chem. Geol.* **2004**, *212*, 255–268.

(19) Bonneville, S.; Behrends, T.; Van Cappellen, P.; Hyacinthe, C.; Roling, W. F. M. Reduction of Fe(III) colloids by *Shewanella putrefaciens*: A kinetic model. *Geochim. Cosmochim. Acta* **2006**, *70*, 5842–5854.

(20) Roden, E. E.; Zachara, J. M. Microbial reduction of crystalline iron(III) oxides: Influence of oxide surface area and potential for cell growth. *Environ. Sci. Technol.* **1996**, *30*, 1618–1628.

(21) Gilbert, B.; Banfield, J. F. Molecular-scale processes involving nanoparticulate minerals in biogeochemical systems. *Mol. Geomicrobiol.* **2005**, *59*, 109–155.

(22) Tang, R. K.; Orme, C. A.; Nancollas, G. H. Dissolution of crystallites: Surface energetic control and size effects. *ChemPhysChem* **2004**, *5*, 688–696.

(23) Lin, S. Y.; Ferg, J.; Biswas, P.; Enzweiler, R.; Boolchand, P. Characterization of maghemite ferric oxide crystals processed by an aerosol technique. *J. Magn. Magn. Mater.* **1996**, *159*, 147–158.

(24) Madden, A. S.; Hochella, M. F. A test of geochemical reactivity as a function of mineral size: Manganese oxidation promoted by hematite nanoparticles. *Geochim. Cosmochim. Acta* **2005**, *69*, 389–398.

(25) Stoscheck, C. M. Quantitation of Protein. *Method. Enzymol.* **1990**, *182*, 50–68.

(26) Stookey, L. L. Ferrozine - a new spectrophotometric reagent for iron. *Anal. Chem.* **1970**, *42*, 779–781.

(27) Snoeyenbos-West, O. L.; Nevin, K. P.; Anderson, R. T.; Lovley, D. R. Enrichment of Geobacter species in response to stimulation of Fe(III) reduction in sandy aquifer sediments. *Microb. Ecol.* **2000**, *39*, 153–167.

(28) Royer, R. A.; Burgos, W. D.; Fisher, A. S.; Jeon, B. H.; Unz, R. F.; Dempsey, B. A. Enhancement of hematite bioreduction by natural organic matter. *Environ. Sci. Technol.* **2002**, *36*, 2897–2904.

(29) Wielinga, B.; Mizuba, M. M.; Hansel, C. M.; Fendorf, S. Iron promoted reduction of chromate by dissimilatory iron-deducing bacteria. *Environ. Sci. Technol.* **2001**, *35*, 522–527.

(30) Lloyd, J. R.; Chesnes, J.; Glasauer, S.; Bunker, D. J.; Livens, F. R.; Lovley, D. R. Reduction of actinides and fission products by Fe(III)-reducing bacteria. *Geomicrobiol. J.* **2002**, *19*, 103–120.

(31) Royer, R. A.; Dempsey, B. A.; Jeon, B. H.; Burgos, W. D. Inhibition of biological reductive dissolution of hematite by ferrous iron. *Environ. Sci. Technol.* **2004**, *38*, 187–193.

(32) Pratesi, G.; Cipriani, C.; Giuli, G.; Birch, W. D. Santabarbaraite: a new amorphous phosphate mineral. *Eur. J. Mineral.* **2003**, *15*, 185–192.

(33) Roden, E. E.; Urrutia, M. M. Influence of biogenic Fe(II)on bacterial crystalline Fe(III) oxide reduction. *Geomicrobiol. J.* **2002**, *19*, 209–251.

(34) Nevin, K. P.; Lovley, D. R. Lack of production of electron-shuttling compounds or solubilization of Fe(III) during reduction of insoluble Fe(III) oxide by *Geobacter metallireducens*. *Appl. Environ. Microb.* **2000**, *66*, 2248–2251.

(35) Liu, C.; Zachara, J. M.; Gorby, Y. A.; Szecsody, J. E.; Brown, C. F. Microbial reduction of Fe(III) and sorption/precipitation of Fe(II) on *Shewanella putrefaciens* strain CN32. *Environ. Sci. Technol.* **2001**, *35*, 1385–1393.

(36) Liu, C. X.; Zachara, J. M.; Zhong, L. R.; Kukkadupa, R.; Szecsody, J. E.; Kennedy, D. W. Influence of sediment bioreduction and reoxidation on uranium sorption. *Environ. Sci. Technol.* **2005**, *39*, 4125–4133.

ES800620F